10-4-2022

A TEM study of Fe_{3+x} $Co_{3-x}Ti_2$ (x = 0, 1, 2, 3) intermetallic alloys

Xingzhong Li

Anandakumar Sarella

B. Balasubramanian

Shah R. Valloppilly

A TEM study of $Fe_{3+x}Co_{3-x}Ti_2$ (x = 0, 1, 2, 3) intermetallic alloys

X.-Z. Li,[1] A. Sarella,[1] B. Balasubramanian,[1,2] and S.R. Valloppilly[1]

1 Nebraska Center for Materials and Nanoscience, University of Nebraska, Lincoln, NE 68588, United States
2 Department of Physics and Astronomy, University of Nebraska–Lincoln, Lincoln, NE 68588, United States

Corresponding author — X.-Z. Li, *email* xzli@unl.edu

Dedicated to D.J. Sellmyer (1938–2022) in memory of his leadership in our research.

Abstract

A TEM study has been carried out on crystal structures in the rare-earth-free intermetallic alloys, $Fe_{3+x}Co_{3-x}Ti_2$ (x = 0, 1, 2, 3). These alloys have been demonstrated to have potentially high magnetic anisotropy. In these alloys, the main intermetallic compound was recently reported as a new hexagonal phase with a space group of P-6 m2. The present study reveals that the main compound belongs to Laves C14 variant surrounded by α-Fe type crystal as secondary phase in the $Fe_{3+x}Co_{3-x}Ti_2$ (x = 0, 1, 2, 3) alloys, in agreement with the Fe-Ti and Fe-Co-Ti phase diagrams. The SAED, EDS, HRTEM and XRD techniques have been carried out to characterize the intermetallic compounds in the $Fe_{3+x}Co_{3-x}Ti_2$ (x = 0, 1, 2, 3) alloys.

Keywords: Fe-Co-Ti, Intermetallic, TEM, EDS, SAED, HRTEM, XRD, Landyne software

Published in *Materials Characterization* 194 (2022) 112366
doi:10.1016/j.matchar.2022.112366

Submitted 9 June 2022; revised 21 September 2022; accepted 29 September 2022; published 4 October 2022.

1. Introduction

Permanent magnets with high remanent magnetization and coercivity (hard magnets) are critical for energy applications such as electric motors and generators. There is an increasing demand for strong permanent-magnet materials due to new trends in the automotive electric car industry. Currently, high-performance hard magnets typically contain rare earth (RE) or precious metals, *i.e.*, $Nd_2Fe_{14}B$ and $SmCo_5$-based materials. Owing to limited RE mineral resources and RE metal supplies, there is a strategic need to discover novel magnet materials containing no or fewer RE elements.

The intermetallic compound in $Fe_3Co_3X_2$ (X = Ti and Nb) alloys [1–4], both were recently reported to be the same type of crystal structure (P-6m2), are the promising compounds for generating high magnetic anisotropy. Zhang et al. [1] reported the atomic structure and magnetic properties of a hexagonal structure investigated by a genetic algorithm (GA), first-principles density functional theory (DFT) calculations, and X-ray powder diffraction (XRD) experiments. The magnetocrystalline anisotropy energy is found to be very sensitive to the occupancy disorder between Fe and Co. Balasubramanian et al. [2] reported the compounds with their composition expanded to $Fe_{3+x}Co_{3-x}Ti_2$ (x = 0, 1, 2, 3), which were referred as to the $Fe_3Co_3Ti_2$-type hexagonal structure with P-6m2 symmetry. Neutron powder diffraction shows a significant Fe/Co anti-site mixing in the $Fe_3Co_3Ti_2$ structure, which strongly affects the magnetocrystalline anisotropy, as revealed by first-principles calculations. Increasing substitution of Fe for Co atoms in the $Fe_3Co_3Ti_2$ lattice leads to the formation of $Fe_4Co_2Ti_2$, Fe_5CoTi, and Fe_6Ti_2 with significantly improved permanent-magnet properties. Xu et al. [3] employed neutron powder diffraction (NPD) to study the detailed crystal structure of $Fe_3Co_3Nb_2$, including the atomic positions and anti-site mixing, taking advantage of the large contrast in the neutron scattering length between Co and Fe. It is confirmed that Co and Fe sites are indeed strongly mixed. Wang, et al. [4] reported the noncollinear spin structure in $Fe_{3+x}Co_{3-x}Ti_2$ (x = 0, 2, 3) from neutron powder diffraction analysis. The nanocrystalline sizes are about 40 *nm* according to the peak width. Projections of the magnetic moment onto both the crystalline *c*-axis and the basal plane were observed and analyzed.

The phase diagrams of the Fe-Ti, Co-Ti and Fe-Co-Ti alloy systems were well investigated and documented [5–9]. The Fe_2Ti is the Laves C14 phase, and Co_2Ti is a Laves C36 phase; both are unique forms of the hexagonal arrangement but share the same basic structure. The structures and magnetic properties of the Fe_2Ti and Co_2Ti Laves phases were reported [10–13]. Fe_2Ti exists in a relatively wide homogeneity range extending from 68.2 to 75.4 *at*.% Fe at higher temperatures and is antiferromagnetic at titanium excess and stoichiometric composition and ferromagnetic at iron excess [10]. It would be interesting to compare the new $Fe_3Co_3Ti_2$ phase to the Laves C14 and C36 phases and their variants.

In the present work, we carried out a TEM study and followed up with XRD on the intermetallic compounds in the $Fe_{3+x}Co_{3-x}Ti_2$ (x = 0, 1, 2, 3) alloys, more detail studies focus on x = 0 and 3 alloys. We discussed the crystal structures based on the selected-area electron diffraction (SAED), energy-dispersive spectroscopy (EDS), and high-resolution transmission electron microscopy (HRTEM), XRD and the Fe-Ti/Fe-Co-Ti phase diagrams. We will show that the main compound in the $Fe_3Co_3Ti_2$ alloy is a variant of a pseudo-binary Laves C14 phase and the structure variation in comparing to the original Laves C14 phase.

2. Material and methods

Samples with nominal compositions of $Fe_{3+x}Co_{3-x}Ti_2$ (x = 0, 1, 2, 3) were fabricated using a conventional arc-melting method followed by a melt-spinning process. First, the alloys with the designed compositions were prepared using the arc-melting process, and homogeneous mixing of elements was obtained by subsequently remelting these alloys five times. Finally, the arc-melted alloys were remelted to a molten stage in a quartz tube in a high-purity argon atmosphere and subsequently ejected onto the surface of a rotating copper wheel with a tangential velocity of 57 ms^{-1} to form ribbons. This non-equilibrium process is used to quench down the compounds in higher temperatures.

The ribbon samples were cut into pieces approximately 2 *mm* long and mechanically ground and polished to approximately 30 μ*m* or thinner. The samples were then mounted onto 3.05 *mm* diameter TEM

Cu rings and milled to electron transparency using a Gatan PIPS II under the conditions of argon ion-beam at 4 *kV*, with an angle starting at 10° and then decreasing to 6°. The TEM, SAED, and HRTEM experiments were carried out on a Thermo Fisher Scientific (former FEI) Tecnai Osiris microscope equipped with a Gatan Orius CCD camera. The microscope operates at 200 *kV* and is equipped with a double-tilt TEM holder. Intermetallic crystal phases were first examined by SAED and EDS analysis and further studied by HRTEM imaging. The EDS data were collected with the ChemiSTEM system on the Osiris microscope and analyzed with Bruker's ESPRIT software. The compositions of the meltspun ribbons were measured using EDS at different locations of the ribbons. The Landyne suite (version 5) was used to simulate and quantify SAED patterns and crystallographic processing of HRTEM images [14]. XRD experiment was carried out on a Rigaku/D Max-B diffractometer with Co Kα radiation (λ = 1.7903 *Å*) using powder samples. The TOPAS (version 5) from Bruker AXS Inc. was used for the XRD refinement [15].

3. Results and discussion

3.1. Magnetic property measurement on $Fe_{3+x}Co_{3-x}Ti_2$ alloys

It is well-known that the magnetic properties of the C14 Laves phase Fe_2Ti with the hexagonal structure show strong composition dependence due to the existence of the energetic near-degeneracy of an antiferromagnetic (AF) and ferromagnetic (FM) ground state. The Fe-Ti alloy has a wide homogeneity range at 1300 °C, leading to the appearance of a composition variant at room temperature for Fe_2Ti. Stoichiometric Fe_2Ti is AF, while Fe-rich $Fe_{2+y}Ti_{1-y}$ ($0.189 \leq y \leq 0.262$) shows FM [11].

In the previous works [1–4], a rare-earth-free magnetic compound in $Fe_3Co_3Ti_2$ alloy and the magnetic properties were investigated, and then the Co was replaced with Fe in $Fe_{3+x}Co_{3-x}Ti_2$ (x = 1, 2, 3) to improve the magnetic properties of the alloys. **Fig. 1** shows (a) the field-dependent magnetization curves of the Fe_5CoTi_2 compound measured at 300 and 10 *K* and (b) Room-temperature hysteresis loops of $Fe_3Co_3Ti_2$, Fe_5CoTi_2, and Fe_6Ti_2. The hysteresis loops reveal higher

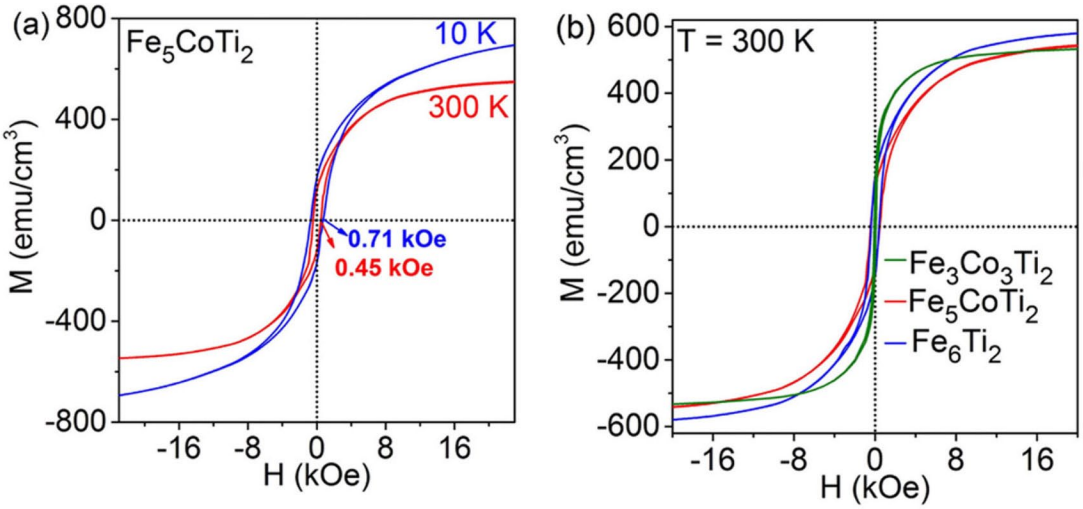

Fig. 1. (a) Field-dependent magnetization curves measured for Fe_5CoTi_2 at 300 *K* and 10 *K*. (b) Room-temperature hysteresis loops of $Fe_3Co_3Ti_2$, Fe_5CoTi_2, and Fe_6Ti_2. [2].

coercivities H_c for Fe_5CoTi_2 (0.45 *kOe* at 300 *K* and 0.70 *kOe* at 10 *K*) as compared to the $Fe_3Co_3Ti_2$ alloy (H_c = 60 *Oe* and 70 *Oe* at 300 *K* and 10 *K*, respectively). The replacement of Co with Fe in the $Fe_{3+x}Co_{3-x}Ti_2$ alloys show increasingly improved properties for permanent magnets [2].

3.2. TEM and EDS results on $Fe_{3+x}Co_{3-x}Ti_2$ (x = 0, 1, 2, 3) alloys

Fig. 2 shows typical morphologies of the microstructures in the $Fe_{3+x}Co_{3-x}Ti_2$ (x = 0, 1, 2, 3) alloys. Two types of morphologies were observed, one in larger grain size as the main compound and the other in smaller grain marked with arrows. In the $Fe_{3+x}Co_{3-x}Ti_2$ (x = 1, 2, 3) alloys, the size of the main grains reaches up to 1 μ*m,* while in $Fe_3Co_3Ti_2$ alloy, the size of the main grains is about 100 *nm*. The chemical compositions of the main compounds are measured from the EDS analysis, as listed in **Table 1**. The secondary phase was found to be Fe-rich (x = 3) or Fe(Co)-rich (x = 0, 1, 2) phases.

According to the phase diagrams of Fe-Ti, as shown in **Fig. 3**, and Fe- Co-Ti (not shown here), the alloy with the compositions of $Fe_{3+x}Co_{3-x}Ti_2$ (x = 0, 1, 2, 3), are in the range of two phases, the Laves C14 type phase and α-Fe BCC type phase. The stoichiometric Laves

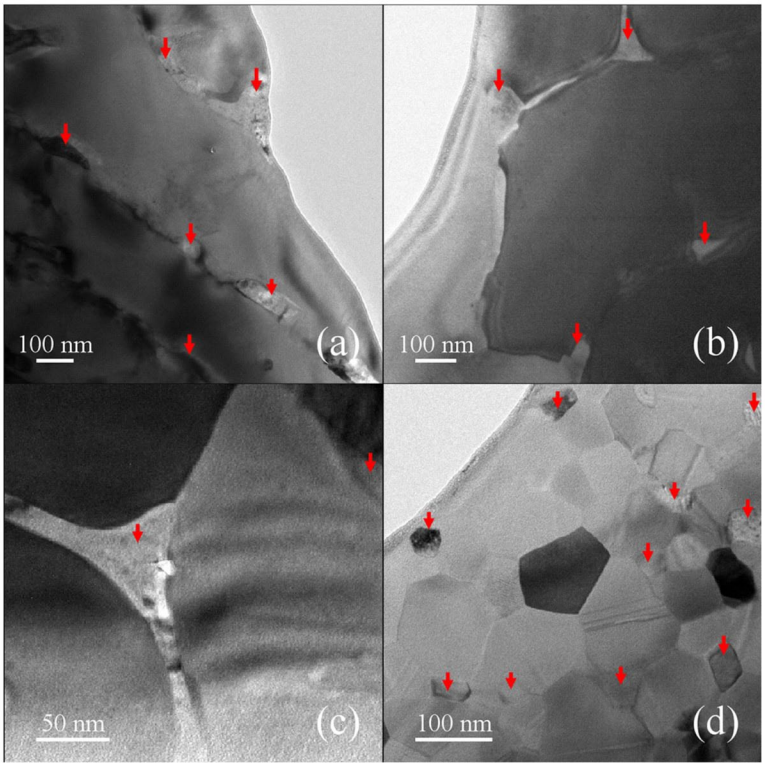

Fig. 2. TEM images of $Fe_{3+x}Co_{3-x}Ti_2$ alloy, (a) x = 3, (b) x = 2, (c) x = 1 and (d) x = 0. The grains of the secondary phase are marked with arrows.

Table 1 EDS results of $Fe_{3+x}Co_{3-x}Ti_2$ alloy x = 0, 1, 2, 3.

Alloy sample (normalized formula)	*Laves C14 variant*
Fe_6Ti_2 ($Fe_{75}Ti_{25}$)	$Fe_{73.5}Ti_{26.5}$ $Fe_{73.9}Ti_{26.1}$
Fe_5CoTi_2 ($Fe_{62.5}Co_{12.5}Ti_{25}$)	$Fe_{61.4}Co_{13.9}Ti_{24.7}$ $Fe_{61.1}Co_{14.7}Ti_{24.2}$
$Fe_4Co_2Ti_2$ ($Fe_{50}Co_{25}Ti_{25}$)	$Fe_{48.4}Co_{24.9}Ti_{26.7}$ $Fe_{47.8}Co_{23.8}Ti_{28.4}$
$Fe_3Co_3Ti_2$ ($Fe_{37.5}Co_{37.5}Ti_{25}$)	$Fe_{35.5}Co_{38.3}Ti_{26.2}$ $Fe_{35.8}Co_{38.9}Ti_{25.3}$

C14 phase is an AB_2 compound that can extend its chemical composition to $A_{1-y}B_{2+y}$ ($y \leq 0.262$ for C14 in Fe-Ti system) in a high-temperature range. We refer hereafter to the compound with a composition of $A_{1-y}B_{2+y}$ ($y \neq 0$) as the variant of the Laves C14 structure.

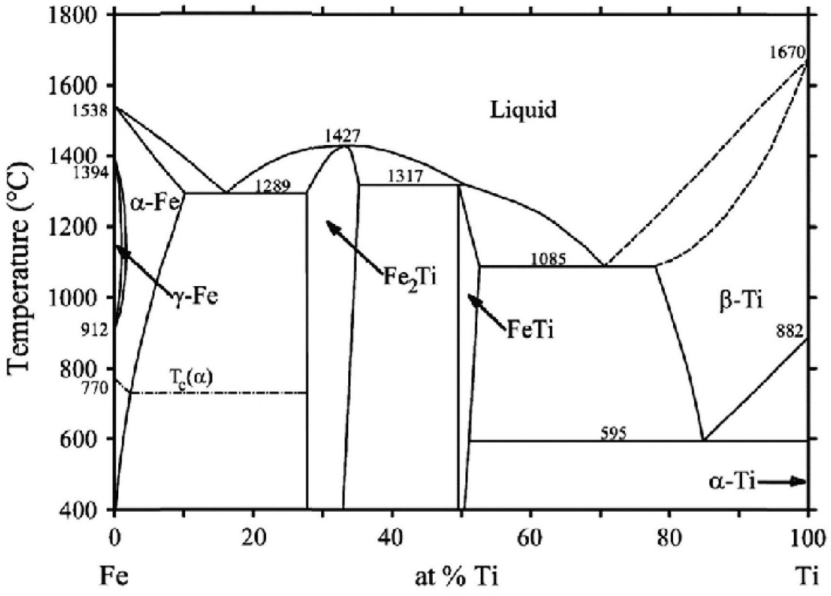

Fig. 3. Phase diagram of Fe-Ti system proposed by Kaufman and Nesor [5].

3.3. SAED results on Fe_6Ti_2 alloy

Fig. 4 shows (a) an experimental SAED pattern taken from the Fe-rich α-Fe BCC type phase in the Fe_6Ti_2 alloy and (b) a simulated SAED pattern with the Fe-rich α-Fe BCC type, a = 2.877 *Å*. Similar SAED patterns were also observed in the $Fe_{3+x}Co_{3-x}Ti_2$ (x = 0, 1, 2) alloys.

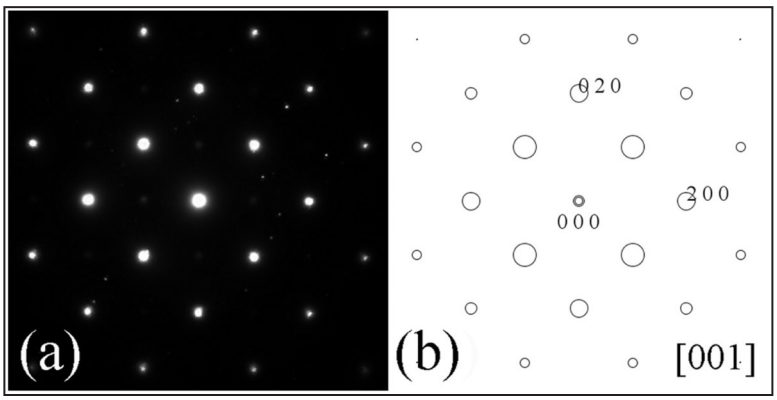

Fig. 4. (a) SAED pattern of the Fe-rich α-Fe BCC type phase and (b) the simulated pattern labelled with the indices and the zone axis.

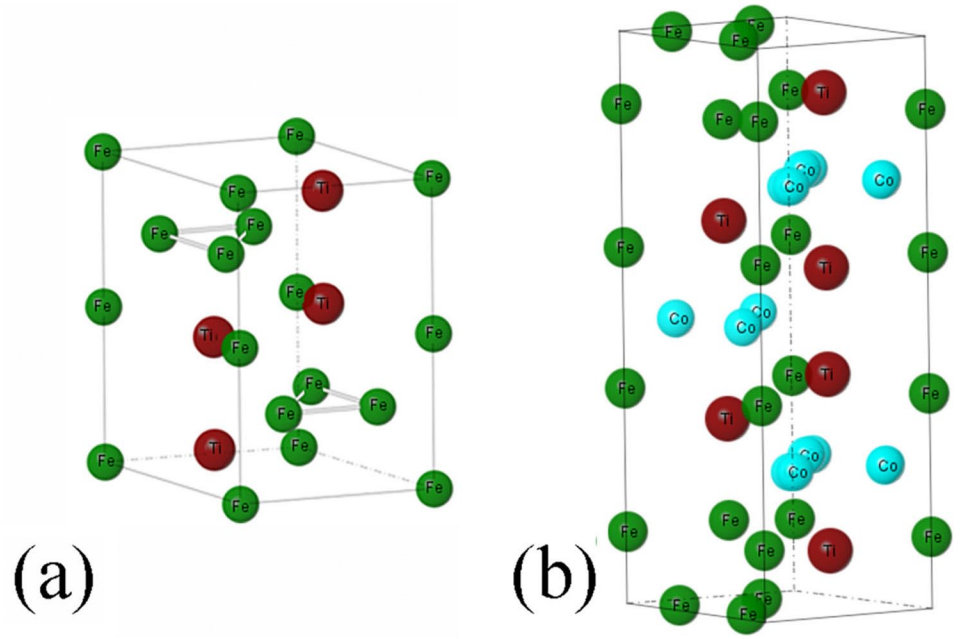

Fig. 5. (a) The crystal structure of Fe_2Ti with a space group of $P6_3/mmc$. (b) The crystal structure of the new $Fe_3Co_3Ti_2$ type with a space group of P-6 m2 [1,2].

Fe_2Ti is the Laves C14 type hexagonal structure (Space group $P6_3/mmc$) with the lattice parameters equaling a = 4.785 *Å* and c = 7.799 *Å*, respectively. **Fig. 5** (a) shows the crystal structure of the Fe_2Ti. There are 4 Ti atoms and 8 Fe atoms in a unit cell. The calculated atomic radius are R_{Ti} = 1.76 *Å* and R_{Fe} = 1.56 *Å*. In the case of an additional insertion of Fe atoms into the stoichiometric lattice, it is conceivable that the larger Tiatoms were statistically substituted by the smaller Fe-atoms (direct substitution). The atomic arrangements in the homogeneity range of the Laves phase Fe_2Ti were investigated using X-ray and neutron diffraction by Brückner et al. [10]. We may indicate the chemical composition in a formula as $Fe_{2+y}Ti_{1-y}$, $y \leq 0.262$. When the Ti atoms were partially replaced by the Fe atoms, the space group $P6_3/mmc$ in the crystal structure may no longer strictly hold.

Fig. 6 shows (a) an experimental SAED pattern from the main compound in the Fe_6Ti_2 alloy and the simulated SAED patterns along the [100] zone axis based on (b) the Fe_2Ti Laves C14 and (c) its variant $Fe_{2+y}Ti_{1-y}$, $y \leq 0.262$. In Fig. 6 (b), the absent reflections along the (001)

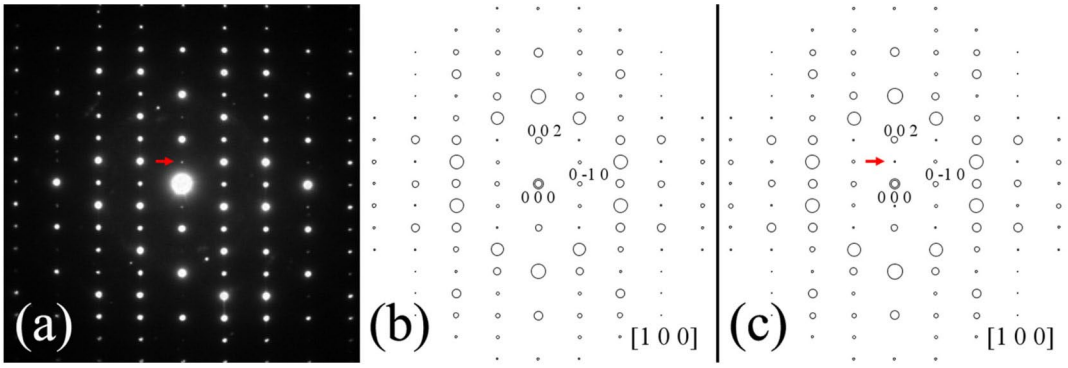

Fig. 6. (a) experimental SAED pattern from the main compound in the Fe_6Ti_2 alloy and the simulated SAED patterns along [100] zone axis based on (b) the Fe_2Ti Laves C14 and (c) its variant $Fe_{2+y}Ti_{1-y}$ $y \leq 0.262$.

row indicate a 6_3 screw-axis. With the more Fe atom in the Fe_6Ti_2 alloy with its composition of $Fe_{2+y}Ti_{1-y}$ $y \neq 0$, the 6_3 screw-axis symmetry is broken, as shown in the arrows in Fig. 6(a) and (c).

3.4. SAED and HRTEM results on $Fe_{3+x}Co_{3-x}Ti_2$ alloys (x = 0,1,2)

SAED patterns and HRTEM images of the samples in the $Fe_{3+x}Co_{3-x}Ti_2$ alloys (x = 0, 1, 2) show no noticeable differences except the grain size difference shown in Fig. 2. Therefore, we focus on the $Fe_3Co_3Ti_2$ sample now. We will compare the variant of the Laves C14 structure and the new $Fe_3Co_3Ti_2$ type proposed by Zhang et al. [1]. Fig. 5 shows the crystal structure of the new $Fe_3Co_3Ti_2$ type in comparison to the Laves C14 Fe_2Ti type. If we consider the sites of Fe and Co atoms are the same type temporarily, then the $Fe_3Co_3Ti_2$ structure can be viewed as two unit-cells of the Laves C14 Fe_2Ti structure bonding together and a pair of original Ti atoms replaced with Fe atoms in mirror positions. Thus, the *c* parameter in the $Fe_3Co_3Ti_2$ type structure is double the *c* parameter of the Laves C14 Fe_2Ti structure.

Fig. 7 shows (a) the experimental SAED pattern of the main compound in the $Fe_3Co_3Ti_2$ alloy and (b) an intensity distribution of the reflections retrieved from the SAED pattern using the Landyne suite. Simulated [100] SAED patterns were carried out based on (c) the Laves C14 variant (this work) and (d) the $Fe_3Co_3Ti_2$ type structure [1,2]. It is clear that the simulated pattern in (c), contrary to the one in (d),

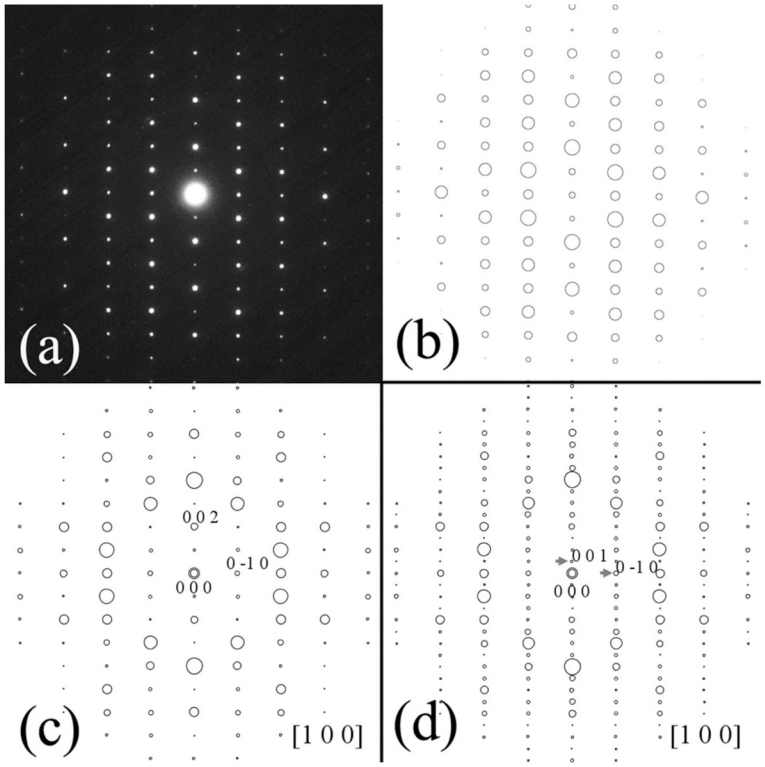

Fig. 7. (a) Experimental SAED pattern of the main compound in the $Fe_3Co_3Ti_2$ alloy, (b) an intensity distribution retrieved from the pattern (a). Simulated SAED patterns based on (c) the Laves C14 variant (this work) and (d) the $Fe_3Co_3Ti_2$ type structure [1,2].

matches well with the experimental pattern in (a) and (b). In addition to the replacement of Ti atoms with partial Fe atoms, the replacement of the Fe with Co breaks even more the 6_3 screw-axis symmetry. This observation is confirmed by the reflections along the (001) row in Fig. 7 (a ~ c).

HRTEM experiment was used to confirm further that the main compound has the crystal structure of the Laves C14 variant in the $Fe_3Co_3Ti_2$ alloy. **Fig. 8** shows (a) the experimental HRTEM image of the main compound in the $Fe_3Co_3Ti_2$ alloy, an FFT pattern is given as inset, and (b) the inverse FFT processing image, in which a unit cell is outlined. The relation between an HRTEM image and the projected crystal potential can be quite complex if the crystal is thick. To obtain an image which can be directly interpreted in terms of projected potential,

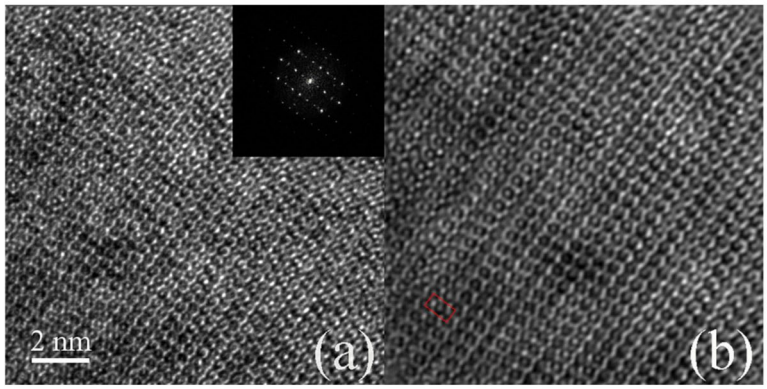

Fig. 8. (a) HRTEM image and (b) the inverse FFT processing image of the main compound in the $Fe_3Co_3Ti_2$ alloy.

the crystals should be well aligned, thin enough to be close to weak-phaseobjects and the defocus value for the objective lens should be optimal, *i. e.* at the Scherzer defocus. The HRTEM image in Fig. 8 can be directly interpreted with the structural projection and the electrostatic potential map of the Laves C14 variant, as shown in **Fig. 9**.

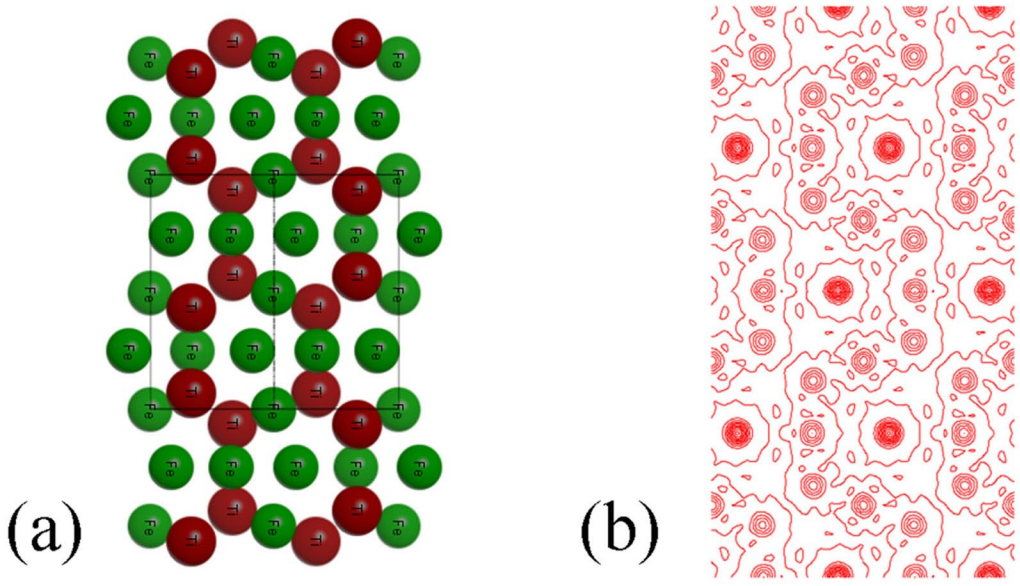

Fig. 9. (a) Structural projection and (b) electrostatic potential map of Laves C14 variant along [100].

3.5. XRD result

The experimental XRD diffractogram has been analyzed by a fitting process based on the structure of Laves C14 variant and the structure proposed by Zhang et al. [1], as shown in **Fig. 10**. It confirms that the $Fe_3Co_3Ti_2$ alloy is composed mainly of a hexagonal intermetallic compound and a small amount of Fe-rich α-Fe type phase, in agreement with the TEM and EDS analysis. The lattice parameters of the hexagonal phase are $a = b = 4.781(1)$ *Å* and $c = 7.784(1)$ *Å* on the Laves C14 variant and $a = b = 4.781(1)$ *Å* and $c = 15.570(1)$ *Å* on the structure proposed by Zhang et al. [1]. The lattice parameters of the Ferich α-Fe type phase are $a = b = c = 2.877(1)$ *Å*. The fit shows about 12 *wt*% of Ferich α-Fe for both structural models of the hexagonal phase. In Fig. 10, the only small difference in the calculated diffractograms based on the two structures appears near 42.5° for the diffractograms with Co Kα radiation spanning from 40° to 100°. Enlarged sections of 40°-45° are embedded in Fig. 10 (a-c). There is no peak from 40°-45° in Fig. 10 (b), which is in agreement with the experimental XRD diffractogram in Fig. 10 (a). However, a small peak (105) appears near 42.5° in Fig. 10 (c). This means that the XRD analysis favors the Laves C14 variant better than the structure proposed by Zhang et al. [1] to be the structure of the hexagonal intermetallic compound in the $Fe_3Co_3Ti_2$ alloy.

3.6. Discussion

The genetic algorithm (GA) [1] is undoubtedly a powerful method for derivation of the new crystal structure. Since unit cell and chemical composition are needed as initial parameters in the method, it will be better if the lattice parameters and chemical composition are allowed to be adjusted during the derivation processing. In the present case, it is important to determine the *c* parameter of the main hexagonal compound in the $Fe_3Co_3Ti_2$ alloy. The TEM and EDS analysis show that the main compound does not fit exactly in the composition of $Fe_3Co_3Ti_2$, which may be better in the formation as $(Fe, Co)_{2+y}Ti_{1-y}$ ($y < 0.262$). Since the $Fe_3Co_3Ti_2$ type structure derived from the GA method is very close to the Laves C14 variant except double the *c* parameter ($15.570/7.784 \approx 2$), it will not alter the main

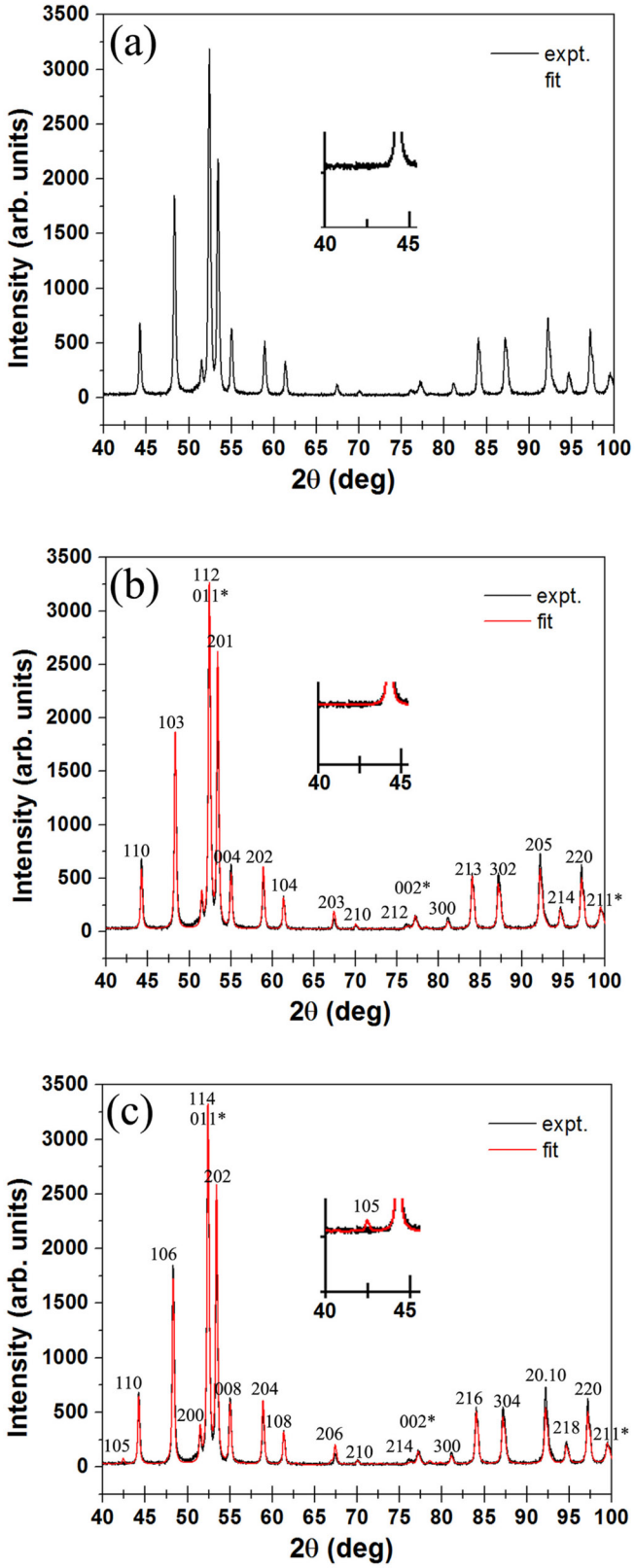

Fig. 10.
(a) The experimental diffractogram of the Fe3Co3Ti2 alloy,
(b) calculated diffractogram on the base of Laves C14 variant, and
(c) calculated diffractogram on the base of the structure proposed by Zhang et al. [1]. Enlarged sections 40°-45° are embedded to show peak details. Peaks of a small amount of Fe-rich α-Fe type phase have also been detected and marked with *.

conclusion in the previous works [1~4]. The present work aims to provide useful information on the structure in further work on this topic.

4. Concluding remarks

The present study provides details on the structural analysis on the rare-earth-free intermetallic alloys, $Fe_{3+x}Co_{3-x}Ti_2$ (x = 0, 1, 2, 3), which have been demonstrated to have potentially high magnetic anisotropy. The SAED, EDS, HRTEM, and XRD results show Laves C14 variant as the main compound, which is surrounded by the Fe-rich α-Fe type secondary phase in $Fe_{3+x}Co_{3-x}Ti_2$ (x = 0, 1, 2, 3) alloys. The conclusion is in agreement with the Fe-Ti/Fe-Co-Ti phase diagrams. Laves C14 variant lost the 6_3 screw-axis symmetry due to the mixing of Fe/Co and Fe/Ti atom sites compared to the original Laves C14 structure with space group, $P6_3/mmc$.

* * * * *

Data availability Data and images analyzed during the current study are available from the corresponding author.

Competing Interest No conflict of interest exists.

Acknowledgments The project was led by Prof. Sellmyer (1938–2022). He passed away before we prepared the manuscript. We would like to dedicate this paper to him in memory of his leadership in our research. The work was performed in part in the Nebraska Nanoscale Facility, National Nanotechnology Coordinated Infrastructure, and the Nebraska Center for Materials and Nanoscience, which are supported by the National Science Foundation under Award ECCS: 1542182 and the Nebraska Research Initiative.

Supplementary data Appendix A follows the **References**.

References

[1] J. Zhang, M.C. Nguyen, B. Balasubramanian, B. Das, D.J. Sellmyer, Z. Zeng, K.- M. Ho, C.-Z. Wang, Crystal structure and magnetic properties of new $Fe_3Co_3X_2$ (X = Ti, Nb) intermetallic compounds, J. Phys. D. Appl. Phys. 49 (2016), 175002.

[2] B. Balasubramanian, B. Das, M.C. Nguyen, X.-S. Xu, J. Zhang, X.-Z. Zhang, Y.- H. Liu, A. Huq, S.R. Valloppilly, Y.-L. Jin, C.-Z. Wang, K.-M. Ho, D.J. Sellmyer, Structure and magnetism of new rare-earth-free intermetallic compounds: $Fe_{3+x}Co_{3-x}Ti_2$ ($0 \le x \le 3$), APL Mater. 4 (2016), 116109.

[3] X.-S. Xu, X.-Z. Zhang, Y.-W. Yin, B. Balasubramanian, B. Das, Y.-H. Liu, A. Huq, D. J. Sellmyer, Anti-site mixing and magnetic properties of $Fe_3Co_3Nb_2$ studied via neutron powder diffraction, J. Phys. D. Appl. Phys. 50 (2017), 025002.

[4] H.-H. Wang, B. Balasubramanian, R. Pahari, R. Skomski, Y.H. Liu, A. Huq, D. J. Sellmyer, X.-S. Xu, Noncollinear spin structure in $Fe_{3+x}Co_{3-x}Ti_2$ (x = 0, 2, 3) from neutron diffraction, Phys. Rev. Mater. 3 (2019) 064403.

[5] L. Kaufman, H. Nesor, Coupled phase diagrams and thermochemical data for transition metal binary systems-I, Calphad 2 (1978) 55–80.

[6] J.L. Murray, Fe-Ti and Co-Ti phase diagrams, in: H. Okamoto, M.E. Schlesinger, E. M. Mueller (Eds.), Volume 3 of the Alloy phase Diagrams, ASM International, Metals Park, OH, 1992.

[7] H. Okamoto, Fe-Ti (Iron-Titanium), J. Phase Equilib. 17 (1996) 369.

[8] T. Kozakai, M. Kobayashi, T. Koyama, M. Doit, T. Miyazaki, Phase diagram of the Fe-co-Ti system at 1073, K Z. Metallkd. 93 (2002) 3.

[9] V. Raghavan, Co-Fe-Ti (cobalt-Iron-titanium), J. Phase Equilib. 24 (2003) 175.

[10] W. Brückner, K. Kleinstück, G.E.R. Schulze, Atomic arrangement in the homogeneity range of the laves phase $ZrFe_2$ and $TiFe_2$, Phys. Status Solidi 23 (1967) 475–480.

[11] W. Brückner, R. Perthel, K. Kleinstück, G.E.R. Schulze, Magnetic properties of $ZrFe_2$ and $TiFe_2$ within their homogeneity range, Phys. Status Solidi 29 (1968) 211–216.

[12] T. Nakamichi, Y. Aoki, M. Yamamoto, Ferromagnetic properties of the intermetallic compound with the hexagonal laves-phase structure in cobalttitanium system, J. Phys. Soc. Jpn. 28 (1970) 590–595.

[13] W.-Y. Zhang, X.-Z. Li, S. Valloppilly, R. Skomski, J.E. Shield, D.J. Sellmyer, Development and intrinsic properties of hexagonal ferromagnetic $(Zr,Ti)Fe_2$, J. Appl. Phys. 115 (2014) 17A769.

[14] Landyne Software Suite in https://landyne.com

[15] TOPAS Software in http://www.topas-academic.net/

Supplementary material

EDS results on alloys with nominal compositions of Fe3+xCo3-xTi2 x = 0, 1, 2, 3

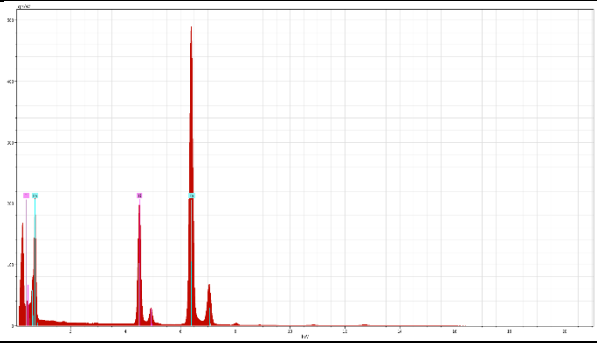	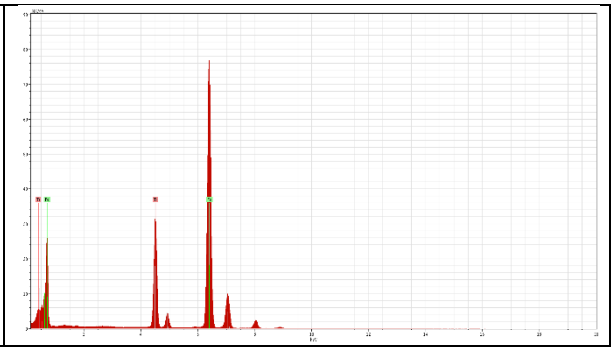
$Fe_{73.5}Ti_{26.5}$	$Fe_{73.9}Ti_{26.1}$
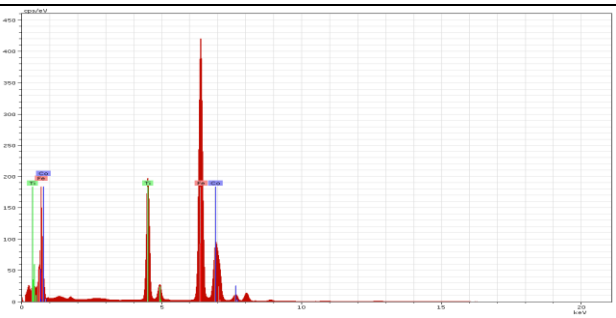	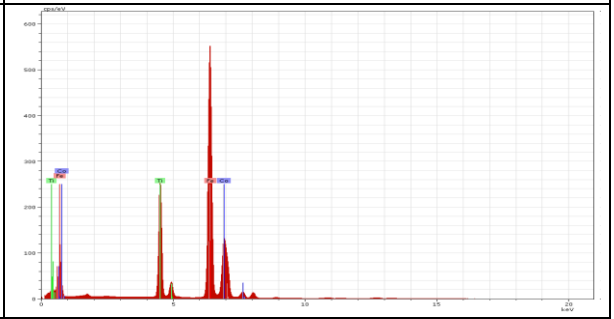
$Fe_{61.4}Co_{13.9}Ti_{24.7}$	$Fe_{61.1}Co_{14.7}Ti_{24.2}$
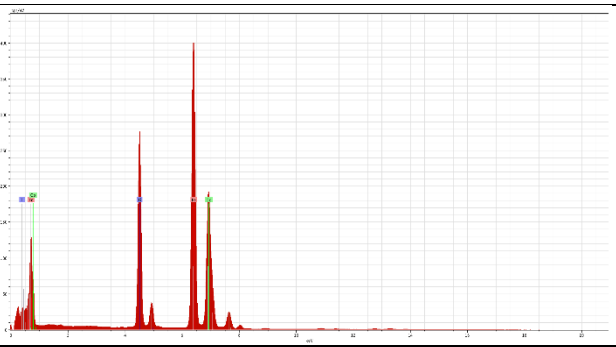	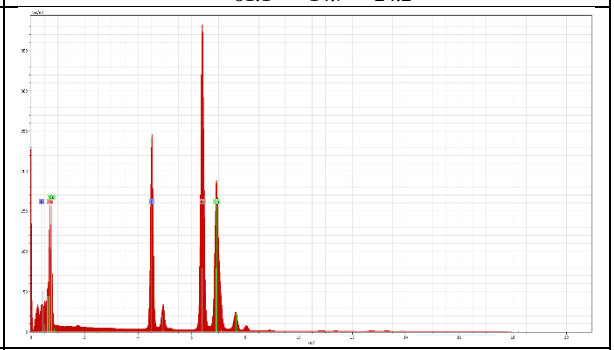
$Fe_{48.4}Co_{24.9}Ti_{26.7}$	$Fe_{47.8}Co_{23.8}Ti_{28.4}$
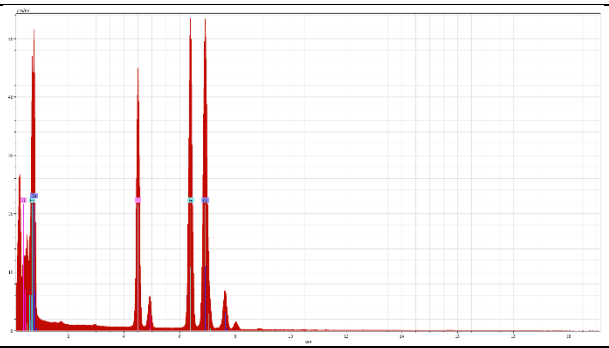	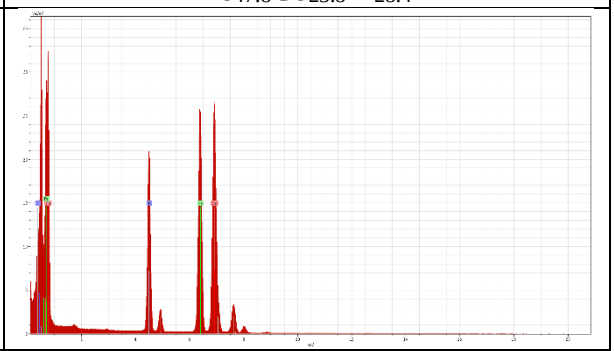
$Fe_{35.5}Co_{38.3}Ti_{26.2}$	$Fe_{35.8}Co_{38.9}Ti_{25.3}$